A bio-inspired polymeric gradient refractive index (GRIN) human eye lens

Shanzuo Ji,[1] Michael Ponting,[1,2,*] Richard S. Lepkowicz,[3] Armand Rosenberg,[4] Richard Flynn,[4] Guy Beadie,[4] and Eric Baer[1]

[1]*Department of Macromolecular Science & Engineering, Case Western Reserve University, Cleveland, Ohio 44106, USA*
[2]*PolymerPlus LLC, Valley View, Ohio 44125, USA*
[3]*Department of Physics and Optical Engineering, Rose-Hulman Institute of Technology, Terre Haute, Indiana 47803, USA*
[4]*Naval Research Laboratory, Code 5616, Washington, DC 20375, USA*
**mponting@polymerplus.net*

Abstract: A synthetic polymeric lens was designed and fabricated based on a bio-inspired, "Age=5" human eye lens design by utilizing a nanolayered polymer film-based technique. The internal refractive index distribution of an anterior and posterior GRIN lens were characterized and confirmed against design by μATR-FTIR. 3D surface topography of the fabricated aspheric anterior and posterior lenses was measured by placido-cone topography and exhibited confirmation of the desired aspheric surface shape. Furthermore, the wavefronts of aspheric posterior GRIN and PMMA lenses were measured and simulated by interferometry and Zemax software, respectively. Their results show that the gradient index distribution reduces the overall wavefront error as compared a homogenous PMMA lens of an identical geometry. Finally, the anterior and posterior GRIN lenses were assembled into a bio-inspired GRIN human eye lens through which a clear imaging was possible.

OCIS codes: (110.2760) Gradient-index lenses; (160.5470) Polymers; (220.1250) Aspherics; (230.4170) Multilayers.

References and links

1. G. Zuccarello, D. Scribner, R. Sands, and L. Buckley, "Materials for bio-inspired optics," Adv. Mater. (Deerfield Beach Fla.) **14**(18), 1261–1264 (2002).
2. R. H. H. Kröger and A. Gislén, "Compensation for longitudinal chromatic aberration in the eye of the firefly squid," Vision Res. **44**(18), 2129–2134 (2004).
3. D. E. Nilsson, L. Gislén, M. M. Coates, C. Skogh, and A. Garm, "Advanced optics in a jellyfish eye," Nature **435**(7039), 201–205 (2005).
4. W. S. Jagger and P. J. Sands, "A wide-angle gradient index optical model of the crystalline lens and eye of the octopus," Vision Res. **39**(17), 2841–2852 (1999).
5. D. E. Nilsson, L. Gislén, M. M. Coates, C. Skogh, and A. Garm, "Advanced optics in a jellyfish eye," Nature **435**(7039), 201–205 (2005).
6. B. Pierscionek, "Species variability in optical parameters of the eye lens," Clin. Exp. Optom. **76**(1), 22–25 (1993).
7. R. C. Augusteyn and A. Stevens, "Macromolecular structure of the eye lens," Prog. Polym. Sci. **23**(3), 375–413 (1998).
8. R. D. Fernald and S. E. Wright, "Maintenance of optical quality during crystalline lens growth," Nature **301**(5901), 618–620 (1983).
9. P. Artal and J. Tabernero, "The eye's aplanatic answer," Nat. Photonics **2**(10), 586–589 (2008).
10. J. F. Koretz and G. H. Handelman, "How the human eye focuses," Sci. Am. **259**(1), 92–99 (1988).
11. Y. Koike, Y. Takezawa, and Y. Ohtsuka, "New interfacial-gel copolymerization technique for steric GRIN polymer optical waveguides and lens arrays," Appl. Opt. **27**(3), 486–491 (1988).
12. T. Zentgraf, Y. Liu, M. H. Mikkelsen, J. Valentine, and X. Zhang, "Plasmonic Luneburg and Eaton lenses," Nat. Nanotechnol. **6**(3), 151–155 (2011).
13. M. Ponting, A. Hiltner, and E. Baer, "Polymer Nanostructures by Forced Assembly: Process, Structure, Properties," Macromol. Symp. **294**(1), 19–32 (2010).

#174652 - $15.00 USD Received 21 Aug 2012; revised 3 Oct 2012; accepted 4 Oct 2012; published 13 Nov 2012

14. G. Beadie, J. S. Shirk, A. Rosenberg, P. A. Lane, E. Fleet, A. R. Kamdar, Y. Jin, M. Ponting, T. Kazmierczak, Y. Yang, A. Hiltner, and E. Baer, "Optical properties of a bio-inspired gradient refractive index polymer lens," Opt. Express **16**(15), 11540–11547 (2008).
15. M. Dubbelman, G. L. Van der Heijde, and H. A. Weeber, "Change in shape of the aging human crystalline lens with accommodation," Vision Res. **45**(1), 117–132 (2005).
16. J. A. Díaz, C. Pizarro, and J. Arasa, "Single dispersive gradient-index profile for the aging human eye lens," J. Opt. Soc. Am. A **25**(1), 250–261 (2008).
17. C. E. Campbell, "Nested shell optical model of the lens of the human eye," J. Opt. Soc. Am. A **27**(11), 2432–2441 (2010).
18. Y. Jin, H. Tai, A. Hiltner, E. Baer, and J. S. Shirk, "New class of bio inspired lenses with a gradient refractive index," J. Appl. Polym. Sci. **103**(3), 1834–1841 (2007).
19. D. A. Atchison and G. Smith, *Optics of the Human Eye* (Butterworth-Heinemann, Leith Walk, 2002), Chap. 1.
20. M. Born and E. Wolf, *Principles of Optics: Electromagnetic Theory of Propagation Interference and Diffraction of Light, 7th Edition* (Cambridge Univ. Press, 2002), Chap. 9.

1. Introduction

Many biological optical systems utilize a gradient refractive index (GRIN) lens, an optic that possess an internal refractive index, to enhance focusing power, increase field of view, and correct for optical aberrations [1]. Biological examples of GRIN lenses include spherical eye lenses found in aquatic creatures such as fish, octopus, squid, and jellyfish [2–5] while aspheric shaped lenses found in air dwellers include humans, lions, and cows [6,7]. In contrast to the compact single or dual lens designs of naturally occurring GRIN eye systems, modern multi-element synthetic lens designs are commonly larger and heavier.

A homogenous glass or plastic spherical singlet lens is the simplest, most compact optic used for imaging. Images produced solely from a single homogeneous lens commonly suffer from significant chromatic and geometrical aberrations [8].The human eye is an optical system consisting of only two lens elements: a cornea and a crystalline lens. Though constructed from only two lens elements, the human eye produces nearly aberration-free imaging [9]. The crystalline human lens functions as an aspheric compensator correcting the corneal induced-spherical aberrations while avoiding any major off-axis coma generation [9]. The superior optical aberration correction of the GRIN lens results from a synergistic dual compensator mechanism comprised of an aspheric lens surface shape and an internal lens GRIN distribution. The refractive index distribution of the human eye lens is constructed of non-planar protein layers, which vary from a maximum refractive index, n = 1.42, at the lens core to a refractive index minimum, n = 1.37, at the lens surface [8, 10]. Constructing a lens with a refractive index distribution shape and magnitude similar to the human eye lens, $\Delta n = 0.05$, requires substantial power and flexibility in materials construction previously unavailable in synthetic optics. Polymeric based GRIN material fabrication techniques, including interface-gel copolymerization [11] and plasmonics [12] approaches have the necessary magnitude in available refractive index gradient, a Δn up to 0.08 is possible; however, they are limited by the internal refractive index distribution control, or the overall lens size due to fabrication techniques, or material diffusion coefficients. Recently, a more flexible alternative to producing polymeric GRIN materials comprised of limitless internal refractive index distribution control was reported based on optic fabricated from nanolayered films [13, 14]. This nanolayered polymers material approach was selected to satisfy the design criteria for producing a polymeric-based, bio-inspired aspheric human eye GRIN lens.

The following work introduces a new material approach that allows for the fabrication of synthetic polymer lenses with geometric and gradient refractive index distributions similar to those of naturally occurring biological animal eyes. A bio-inspired example which utilizes nanolayered polymer films to fabricate an aspheric shaped GRIN lens with the shape and magnitude of a refractive index distribution modeled from a (chronologically equivalent, "Age=5") human lens was fabricated. This work represents the first published attempt to produce a synthetic copy of an aspheric GRIN synthetic eye lens with a geometry and refractive index distribution similar to those of the human eye lens.

#174652 - $15.00 USD Received 21 Aug 2012; revised 3 Oct 2012; accepted 4 Oct 2012; published 13 Nov 2012

2. Design of a bio-inspired human eye lens

Though the geometry of an aging human eye has been extensively studied and reported by several independent sources [15–17], an optical design for constructing a synthetic, bio-inspired version of the human eye GRIN anterior and posterior lens was based on the geometry and an internal refractive index profile reported by Díaz et al. [16]. In this work, Díaz provides a complete description of age dependent eye geometry as well as the internal human eye lens refractive index distribution profile accounting for age-dependent vision deterioration and eye chromatic aberrations [16]. As a result of human growth and age-related lens deterioration, an optical copy of the human eye is a function of age. To fabricate a bio-inspired GRIN lens, described by the Díaz model in Eq. (1), an age dependent lens thickness and surface curvature relationship for a rotationally symmetric concoid lens shape was utilized.

$$d_{L.}(mm) = 2.93 + 0.236 \times age \tag{1}$$

The curvature radii of anterior, Eq. (2), and posterior, Eq. (4), human eye lenses, as well as their aspheric shape coefficient, are given by Eqs. (3) and (5), respectively.

$$R_{anterior}(mm) = 12.7 - 0.058 \times age \tag{2}$$

$$Q_{anterior} = -5 \tag{3}$$

$$R_{Posterior}(mm) = -5.9 - 0.0015 \times age \tag{4}$$

$$Q_{posterior} = -4 \tag{5}$$

The crystalline lens was considered as one element with a single continuous GRIN distribution and its refractive index distribution given by

$$n(\lambda, x, y, z) = n_0(\lambda) + n_1(\cos(n_2 z) - 1) + n_3 \sin(n_4 z) + n_5(x^2 + y^2) \tag{6}$$

Here, z represents the lens optical axis; with $x^2 + y^2$ modeling the elliptical shape of the isoindicial surfaces, and the function sin accounts its asymmetry along the lens axis.

Adopting the "Age=5" human eye lens design maximized the magnitude of the internal lens refractive index distribution, however, any age human eye lens and refractive index distribution could have been fabricated. The "Age=5" lens was, therefore, selected as an initial materials capability demonstrator of the nanolayered polymer GRIN lens fabrication technique flexibility.

A ray tracing model based on the geometry and internal refractive index distribution of the "Age=5" GRIN lens was created in Code V software, to verify the refractive index with Diaz's published model, as shown in Eq. (6) and Fig. 1. The spherical, rather than ellipsoidal contours of the model capture the salient optics of the nested protein layers while allowing for improved computational and fabrication efficiency. Large differences due to the different geometries would be expected only for rays entering at the edges of the lens, which would be blocked by the iris in all but dark conditions. The polynomial coefficients used in this model are listed in Table 1.

$$n(r) = n_0 + n_1(r - R) + n_2(r - R)^2 + n_3(r - R)^3 + n_4(r - R)^4 \tag{7}$$

$$\text{Where } r = \frac{R}{|R|}\sqrt{x^2 + y^2 + (R - z)^2} \tag{8}$$

Table 1. Polynomial Coefficients of an "Age=5" Human Eye Lens Used in Code V Model

Lens	n_0	n_1	n_2	n_3	n_4
Anterior	1.3680	–0.0817	–0.0280	0.0075	0.0031
Posterior	1.4190	0.0006	–0.0300	0.0100	–0.0012

#174652 - $15.00 USD Received 21 Aug 2012; revised 3 Oct 2012; accepted 4 Oct 2012; published 13 Nov 2012

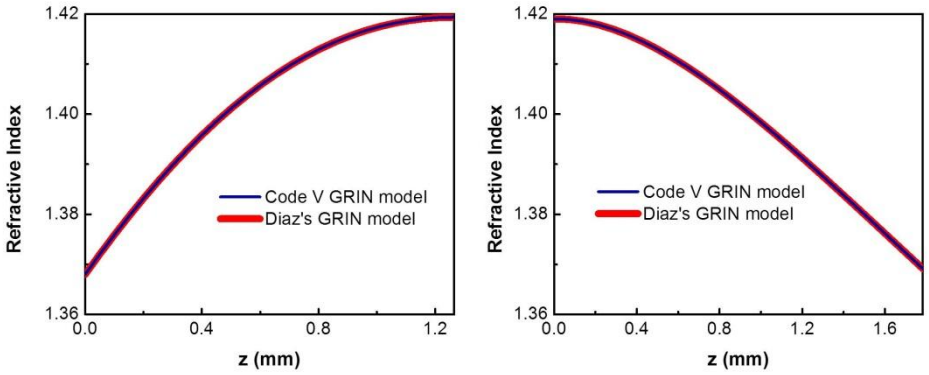

Fig. 1. Refractive index distribution of the anterior and posterior lenses of an "Age=5" human eye lens represented in the Diaz's and Code V models.

Fabricating a nanolayered polymer film-based GRIN lenses required two alternations to Diaz's model: (1) segmentation of the bi-convex human eye lens into two plano-convex GRIN halves that resulted in the creation of anterior and posterior parts segmented at the maximum internal refractive indexes of the lens, Fig. 2(a), and (2) utilizing existing coextruded PMMA/SAN17 nanolayered optical film, with an available range of refractive index from 1.489 to 1.573 as compared to the internal 1.37 to 1.41 biological refractive index distribution of the human eye. To compensate for the difference in the biological and polymer material refractive index, the internal refractive index design of the "Age=5" lens was offset by a refractive index of + 0.12 as shown in Fig. 2(b). Since this offset existed, and because the lens was tested in air, rather than the naturally occurring aqueous environment, holding the lens to its naturally occurring shape would result in blurred test images. As such, the polynomial coefficients for the bio-inspired anterior and posterior lenses, Table 2, was utilized.

Table 2. Polynomial Coefficients of the Bio-inspired Anterior and Posterior Lenses

Lens	n_0	n_1	n_2	n_3	n_4
Anterior	1.4890	–0.0817	–0.0280	0.0075	0.0031
Posterior	1.5403	0.0006	–0.0300	0.0100	–0.0012

The lens surfaces were optimized independently of their original shape for better in-air imaging. The optimization was performed at a single wavelength (the d-line at 587.6 nm) and used on-axis light. The improved performance represented by Fig. 2(c) was obtained with radii curvatures of 12.40 and –5.90 mm, respectively, for the anterior and posterior lens surfaces. Furthermore, an aspheric conic constant was adopted for each surface, with values of 0.5 (anterior) and –5.0 (posterior). Results from these values result in a simulated monochromatic, diffraction-limited performance on-axis, with off-axis aberrations dominated by coma. This change was not a required design change based on material nor fabrication limitations, but was a conscious decision by the authors to display an aspheric GRIN optic capable of evaluation in a conventional air based, n = 1.0, laboratory environment.

#174652 - $15.00 USD Received 21 Aug 2012; revised 3 Oct 2012; accepted 4 Oct 2012; published 13 Nov 2012

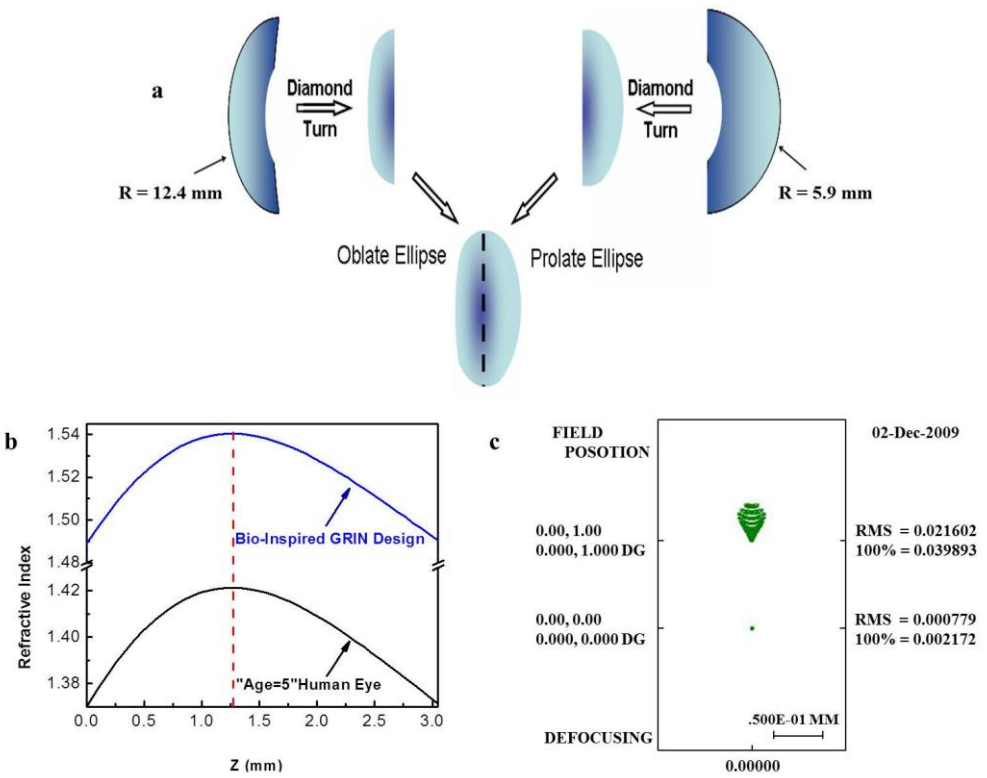

Fig. 2. Design of a bio-inspired polymeric gradient refractive index (GRIN) human eye lens. a) Fabrication illustration to create the bio-inspired GRIN anterior and posterior lenses. b), refractive index distribution of "Age=5" human eye and buildable bio-inspired GRIN lenses. c), RMS wave error of bio-inspired GRIN lenses with two different sets of aspheric coefficient for anterior and posterior lenses simulated by Zemax software: (Top) $Q_{anterior} = -5$, and $Q_{posterior} = -4$; (Bottom) $Q_{anterior} = 0.5$, and $Q_{posterior} = -5$.

3. Experimental

Utilizing the nanolayered polymer coextrusion technique, a set of transparent polymer films, each with a specified refractive index, were fabricated. Each film contains 4097 alternating layers of PMMA and SAN17 with individual layer thickness less than a quarter of visible lights wavelength as previously described [13, 14]. A series of 51 compositions of nanolayered films, differing in refractive index by about 0.0016, were produced by systematically varying the constituent ratios during coextrusion. Each nanolayered film had a thickness of approximately 50 ± 4 μm. The nanolayered films were extruded with protective peel-off layers of low density polyethylene, which improved the surface quality of these films and made it easier to exclude contaminants during the stacking process [14].

Based on the synthetic eye lens design refractive index distribution, 1.49 to 1.54 (see Fig. 3), anterior and posterior lens sheets were stacked from 64 and 76 individual 50 μm nanolayered films, respectively, in a class 10,000 clean room. Nanolayered films were selected based on a closest match refractive index with the design refractive index distribution. The nanolayered film stacks of the anterior and posterior GRIN distribution were thermoformed into 2.6 and 3.1 mm thick GRIN sheets in a heated hydraulic compression molder at 135 °C and 17,000 lb_f.

#174652 - $15.00 USD Received 21 Aug 2012; revised 3 Oct 2012; accepted 4 Oct 2012; published 13 Nov 2012

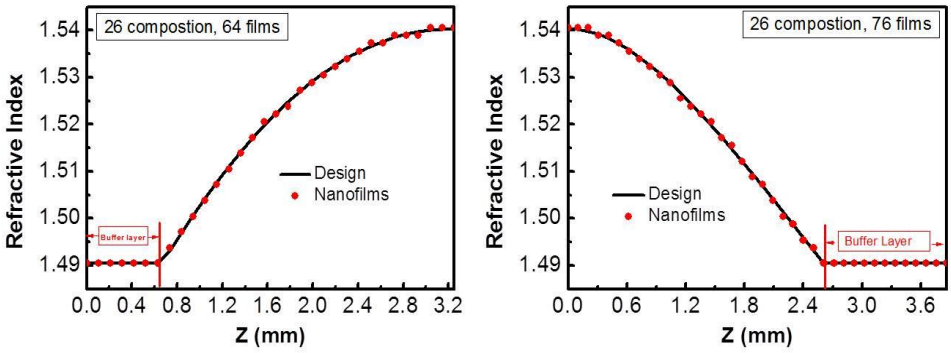

Fig. 3. Stacking recipes of anterior (left) and posterior (right) lens sheets with buffer layers.

The anterior and posterior GRIN sheets were shaped into spherical pre-forms in a compression press against a pair of convex and concave glass lenses with radii of 10.9 and –12.4 mm, as well as, 3.3 and –5.9 mm, respectively, at 130°C and 500 lb_f. After thermoforming, the spherical anterior and posterior lens pre-forms were diamond turned into the prescribed aspheric surface shape.

The wavefront measurements were performed with a commercial sensor based on lateral shearing interferometry, with a maximum 3.6 mm diameter aperture sampled at 120 x 120 points. The test lenses were placed in a broad area collimated laser beam with a 633 nm wavelength, far enough away from the sensor to focus the light in air and have the beam expand back up to a 3 mm diameter in the measurement plane. Over the full aperture of the lenses, the aspheric coefficients were high enough to create caustics near the edges of the beam. To combat this effect, irises placed before the test lenses reduced the input beam diameters to slightly under the radii needed to ensure smooth intensity variations for wavefront analysis. The apertures reduced the beam diameters to 80% of the full lens diameters. The aperture sizes were taken into account in the comparisons between data and simulations.

4. Results and discussion

In a previous work, it was reported that the PMMA/SAN17 spherical GRIN lens exhibited better optical performance than commercial glass singlets in terms of energy concentration and image quality [13, 14]. Here, fabricated aspheric anterior and posterior GRIN lenses were characterized to determine geometric and optical compliance against the Code V model. Characterizing the anterior and posterior lens included the following: (1) verification of the internal lens refractive index distribution and shape, (2) an aspheric surface curvature measurement, (3) wavefront measurements, and (4) an imaging test collected through the bonded GRIN lens.

To ensure the stacked and compressed GRIN sheet contained the desired refractive index distribution, the refractive index distribution in both of the anterior and posterior lens blanks were characterized by a μATR-FTIR examination by exhuming cross sections of adjacent sheet material. The μATR-FTIR technique can map the relative composition across the cross-sectioned sheet surface, which is directly related to the refractive index distribution of the piece [18]. A plot of the design and μATR-FTIR-measured GRIN sheet refractive index distribution displays good agreement with the fabricated anterior and posterior GRIN sheets, shown in Fig. 4.

#174652 - $15.00 USD Received 21 Aug 2012; revised 3 Oct 2012; accepted 4 Oct 2012; published 13 Nov 2012

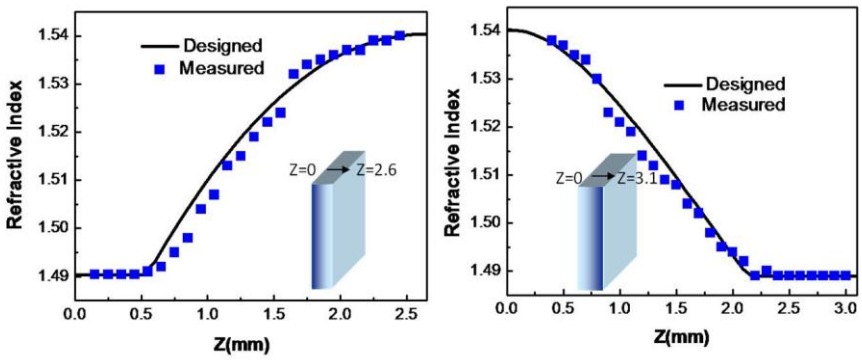

Fig. 4. Refractive index distribution of anterior (left) and posterior (right) lens sheets measured by μATR-FTIR.

An image and 3D profile of the fabricated aspheric anterior and posterior GRIN lens are shown in Figs. 5(a) and 5(d). For this lens, the surface profiles satisfy the Eq. (6) below [19],

$$h^2 + (1+Q)z^2 - 2zR = 0 \tag{9}$$

Where $h^2 = x^2 + y^2$,the z axis is the optical axis, R is the vertex radius of curvature, and Q is the surface aspheric coefficient. Cross-sectional profiles of an aspheric lens and a spherical lens with consistent geometries as the aspheric anterior and posterior GRIN lens were calculated and plotted in Figs. 5(c) and 5(f). These values show good agreement between the measured profiles of aspheric anterior and posterior GRIN lenses and calculated profiles.

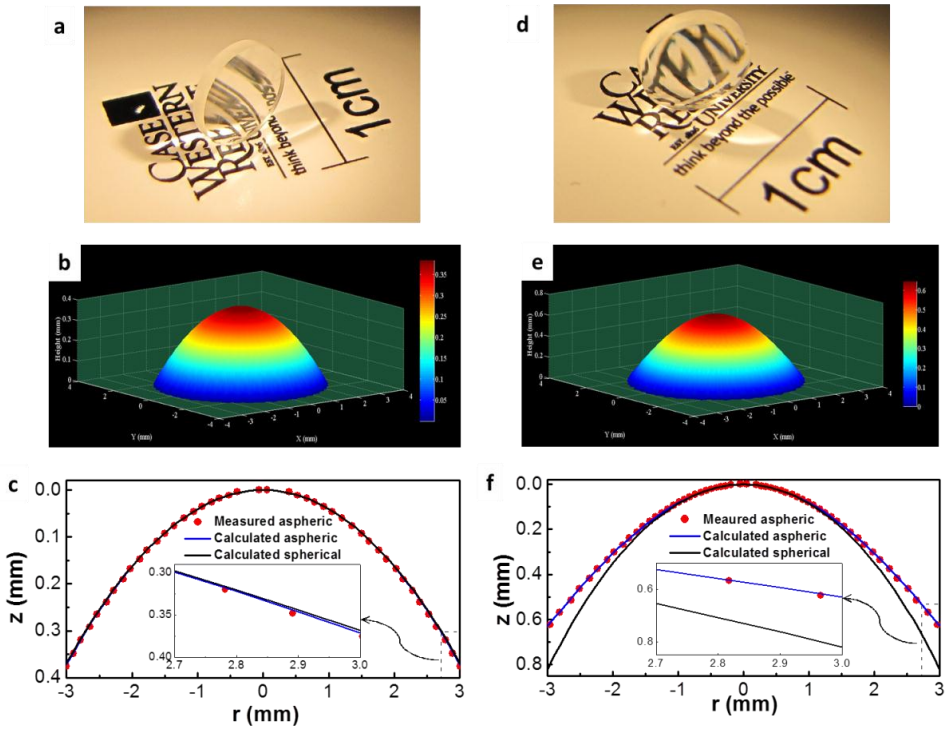

Fig. 5. Fabricated lens images (a and d) and measured geometry surface profiles (b/c and e/f) of the aspheric anterior and posterior bio-inspired human eye GRIN lenses.

#174652 - $15.00 USD Received 21 Aug 2012; revised 3 Oct 2012; accepted 4 Oct 2012; published 13 Nov 2012

Optical wavefront measurements were conducted on the posterior GRIN lens and tested with light incident to the planar lens surfaces, i.e. from the same direction as their design. Figure 6(a) shows the wavefront measured at the sensor plane after the posterior GRIN lens, next to Fig. 6(b), which predicts a theoretical ray trace through the design lens at the same location. Both wavefronts were fit to a series of Zernike polynomials [20].These results were plotted in Fig. 3(b) and represent the residual wavefronts after low-order terms for offset, tilt, and power were subtracted. In the lens design there were no contributions due to tilt. However, in the measured lens there were tilt contributions at the sensor plane of 7.6 waves (peak-to-valley) across the field of view, indicative of the level of parallelism achieved in the diamond turning process. The remaining data show excellent agreement between the measured and predicted wavefronts. Qualitatively the shapes are the same, and quantitatively the wavefronts agree to within a RMS error of 0.10 waves.

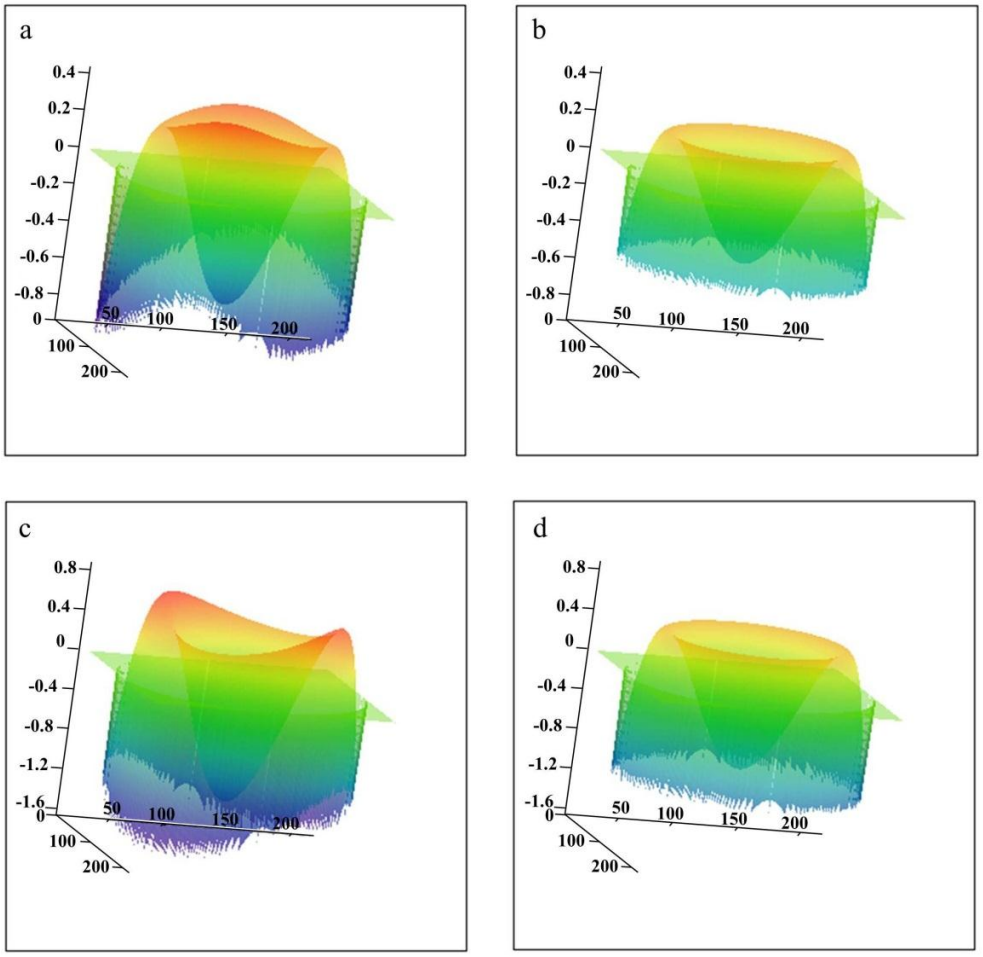

Fig. 6. Comparison plot of experimentally measured and simulated wavefront for as built bio-inspired aspheric posterior lenses. a-b, Measured (a) and numerical simulated (b) wavefront of aspheric posterior GRIN lens. c-d, Measured (c) and numerical simulated (d) wavefront of aspheric posterior PMMA reference lens. Vertical axis in units of waves (633nm). Planar values are unit less measures of aperture across the wavefront sensor.

Figures 6(c) and 6(d) show analogous wavefront data for the non-GRIN, PMMA version of the posterior lens, but are displayed with different vertical scales to Figs. 6(a) and 6(b). Designed to the same shape as the GRIN lens, differences between the two highlight the

#174652 - $15.00 USD Received 21 Aug 2012; revised 3 Oct 2012; accepted 4 Oct 2012; published 13 Nov 2012

effect of the gradient index distribution on the wavefront. As can be seen from a comparison between Figs. 6(d) and 6(b), the gradient index distribution reduces the overall wavefront error. The RMS wavefront error is reduced by the gradient index distribution from 0.41 down to 0.20 waves. A surface figure error in the diamond turned PMMA part produced a radial asymmetry in the measured wavefront, shown in Fig. 6c. Subtracting the tilt contribution to the wavefront, shown in Fig. 6(c), produced 18.8 waves, peak-to-valley, across the measured aperture. The wavefronts displayed in Figs. 6(c) and 6(d) agree to one another within a RMS variation of 0.18 waves.

The aspheric anterior and posterior GRIN lenses were reversibly assembled into a human eye lens. This lens captured an image of Case Western Reserve University logo, shown in Fig. 7. The image was clear and sharp, confirming the focusing ability of the singlet, bio-inspired human eye lens. As expected from the design, on-axis imaging is seen to be superior to off-axis imaging in the figure.

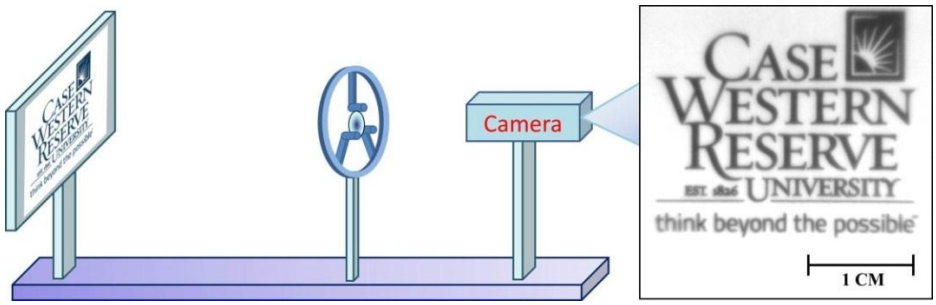

Fig. 7. Experimentally obtained image of a Case Western Reserve University logo taken through a bio-inspired "age=5" human eye GRIN lens. The logo was placed about 33 cm from a bare CCD camera. The Case logo was laser printed onto standard letter paper, illuminated by an external light source, and imaged onto the camera by a bio-inspired "age=5" human eye GRIN lens.

5. Conclusion

The design and fabrication flexibility afforded by the nanolayered film-based GRIN lens technology enabled successful demonstration of an "Age=5" bio-inspired, aspheric human eye GRIN lens. Characterizing the polymer lenses demonstrated an ability to fabricate the nanolayered polymer materials to an external aspheric design shape, with an internal refractive index distribution to specification. Demonstrated in the design of the human eye GRIN lens, are additional freedoms, previously unavailable to optical designers, but available with this technology. The ability to independently select arbitrarily shaped refractive index distributions and optic surface shapes, spherical or aspheric, allows for advances and potential element reductions in modern high resolution and complex zoom, optical systems. Though a first generation design, the polymeric nanolayered GRIN lens technology, demonstrated in this work, enables many potential advances toward fabrication of more compact optical systems, similar to one or two lens biological systems. Other opportunities to apply this technology include lightweight, miniaturized imaging or surveillance systems, conventional glasses, contacts, or potentially customizable gradient refractive index distribution lens implants.

Acknowledgments

This research was supported by the NSF Center of Layered Polymeric Systems (Grant DMR-0423914) and the Defense Advanced Research Projects Agency (Contract HR0011-10-C-0110).

#174652 - $15.00 USD Received 21 Aug 2012; revised 3 Oct 2012; accepted 4 Oct 2012; published 13 Nov 2012